Quantifying Landfill Emission Potential Using a Weakly Coupled Particle Filter

Wang, L.; Heimovaara, T. J.

DOI
10.1029/2023WR036549

Publication date
2025

Document Version
Final published version

Published in
Water Resources Research

ADVANCING EARTH AND SPACE SCIENCES

Water Resources Research

RESEARCH ARTICLE
10.1029/2023WR036549

Key Points:

- A new weakly coupled particle filtering method on a travel time distribution model is used for landfill emission potential estimation
- Analysis clearly demonstrates added value derived from assimilating both leachate production rate and concentration measurements
- The effectiveness of data assimilation is maximized when the measurable state exhibits a strong sensitivity to the pertinent hidden state

Correspondence to:
L. Wang,
l.wang-10@tudelft.nl

Citation:
Wang, L., & Heimovaara, T. J. (2025). Quantifying landfill emission potential using a weakly coupled particle filter. *Water Resources Research*, *61*, e2023WR036549. https://doi.org/10.1029/2023WR036549

Received 24 OCT 2023
Accepted 23 JAN 2025

Author Contributions:
Conceptualization: L. Wang, T. J. Heimovaara
Formal analysis: L. Wang
Funding acquisition: T. J. Heimovaara
Investigation: L. Wang
Methodology: L. Wang
Project administration: T. J. Heimovaara
Resources: L. Wang
Software: L. Wang
Supervision: T. J. Heimovaara
Validation: L. Wang
Visualization: L. Wang
Writing – original draft: L. Wang
Writing – review & editing: T. J. Heimovaara

Quantifying Landfill Emission Potential Using a Weakly Coupled Particle Filter

L. Wang[1] and T. J. Heimovaara[1]

[1]Department of Geoscience and Engineering, Faculty of Civil Engineering and Geosciences, Delft University of Technology, Delft, The Netherlands

Abstract The emission potential, which represents the total leachable mass in landfill waste body, is hard to measure directly. Therefore we propose to quantify it by assimilating available measurements. The leachate production rate is influenced by the total water storage in the waste body, while both total chloride mass and total water storage in the waste body influence the chloride concentration in the leachate. Thus assimilating leachate volume and chloride concentration simultaneously will help quantify the uncertainties in emission potential. This study investigated the feasibility of using a particle filter in a concentration-volume coupled travel time distribution model to estimate the emission potential. Leachate production rates and chloride concentrations were assimilated simultaneously by a weakly coupled data assimilation method. The time lag issue in the travel time distribution model was solved by adding a daily model error to cover layer states. The proposed method was tested in synthetic experiments first to investigate the performance. The results show that the uncertainties in chloride mass and waste body total water storage were quantified and reduced. The predictions of chloride concentrations were also improved.

Plain Language Summary This study presents a method for estimating the amount of harmful chloride in landfill waste and predicting leachate emissions. By combining measurements of water flow (leachate production rate) and chloride concentration, we improved our understanding of total water storage and chloride mass in the waste. Our approach performed best when both measurements were assimilated, and the leachate production rate was sensitive to the variations in water storage within the waste body. The method showed promise in estimating both water storage and chloride mass with correct model parameters, paving the way for future research on understanding uncertainties caused by model parameters.

1. Introduction

Municipal solid waste (MSW) landfill leachate is a primary source of pollution to the surrounding environment because it is a source of contamination for soil and groundwater (Brand, 2014; Fatoba et al., 2021; Gworek et al., 2016). The environmental risk of leachate is determined by its composition and the amount released to the environment. The leachate flux from old landfills is mainly controlled by the water balance of the landfill which depends on precipitation and evapotranspiration. Leachate composition is influenced by the water storage and pollutant mass present in the waste body (Grugnaletti et al., 2016; Laner et al., 2011; Yang et al., 2015). Also, reliable predictions of leachate emissions in the long term require a quantitative assessment of total pollutant mass and water storage in the waste body. As such, this quantitative assessment is an important criterion to determine the aftercare strategy (Kattenberg & Heimovaara, 2011).

Direct measurement of pollutant mass and water storage is virtually impossible due to the size and heterogeneity of waste bodies. As a result, researchers have developed alternative approaches that use forward modeling to predict leachate flux, composition, and the evolution of pollutant mass and water storage over time. For instance, Pantini et al. (2014) developed a process-based landfill water balance model where biodegradation and waste compression processes are included. Grugnaletti et al. (2016) got more accurate leachate production predictions by carrying out a parameter calibration with available outflow measurements. J. Zhang et al. (2021) proposed a pollutant concentration, leakage rate, and a solute transport coupled model that allows the prediction of concentrations. Generally, initial values of water and pollutant storages in the models are often approximated by waste characteristics like waste initial moisture (São Mateus et al., 2012; Yang et al., 2015). However, these estimations could be biased because of the significant spatial variation in initial states and the lack of information on waste composition. Laboratory studies help quantify certain model parameters, but small-scale tests often fail to capture the behavior of full-scale landfills (Fellner et al., 2009). Even when initial moisture levels are calibrated with observations, as in Grugnaletti et al. (2016), the results reflect an averaged value of the whole waste body. While these models can reasonably predict leachate production rates, they struggle to capture the dynamics of pollutant concentration in leachate.

It is generally known that the contaminants are leached out from waste through preferential flow (Fellner & Brunner, 2010). It means we may not need to explicitly consider the heterogeneity of waste properties if we can use a function to describe the preferential flow. Recent research shows that travel time distributions can be used to characterize the flow pathway heterogeneity (Rinaldo et al., 2011). We have developed a travel time distribution (TTD) model to predict leachate production rate (LPR) and chloride concentration from landfill waste bodies (Heimovaara & Wang, 2024). The preferential water flow in landfill waste bodies is primarily characterized by two travel time distributions: one for infiltration from the cover layer and another for baseflow from bulk storage. The concentration states in this model are one-way coupled to the water volume states, meaning changes in concentration levels are controlled by changes in water volume. Parameters and initial states in this model are obtained by optimization using the DREAM$_{zs}$ algorithm (Vrugt, 2016), a Markov chain Monte Carlo (MCMC) method for Bayesian inference.

In recent years, MCMC methods have been widely applied to hydrology models. It allows for estimating the probability distribution of model parameters by comparing model results with available measurements. However, obtaining parameters by fitting or "history-matching" to data is generally a batch processing method that defines the best fit in an average way. This implies that we get the best fit of the measured data over the whole time range rather than the best estimation of model states (Liu & Gupta, 2007). Hence, normal MCMC-like batch processing methods cannot recursively include new information when it becomes available.

Data assimilation (DA) is another class of Bayesian inference methods. It is widely used because of its power to recursively assimilate new measurements to improve understanding of immeasurable or hidden states (Carrassi et al., 2018; Liu et al., 2012). Most DA algorithms consist of alternating forecast and analysis steps. Model states are propagated with time using a forward model to get predictions, and then measurements are used to update the predictions in analysis steps. This sequential updating allows model states to be refined whenever new observations become available.

Filter and smoother are two main categories of data assimilation. Filters estimate current states using past and current observations, making them efficient for real-time applications. On the other hand, Smoothers use both past and future observations to improve accuracy but are more computationally demanding. For example, the ensemble Rauch-Tung-Striebel smoother (EnRTSS) (Raanes, 2016) leverages batch processing to recursively update states, making it suitable for retrospective analysis. Since our objective is to update model states once new observations are available, we focus on the more computationally efficient filtering methods.

Among the main data assimilation filtering methods, the ensemble Kalman filter (EnKF) (Evensen, 2003) and the particle filter (PF) (Djurić et al., 2003) are commonly used for nonlinear forward models. The state update performed by the EnKF is an affine transformation that is precise only when the joint distribution of states and observations follows a multivariate Gaussian distribution. If it isn't, the update is only approximate and can violate all manner of physics. In contrast, particle filtering approaches can preserve the physics because the measurements are used to weigh particles instead of adjusting them. Due to its ability to handle fully nonlinear systems, it has been widely used in hydrology (Abbaszadeh et al., 2019; Plaza Guingla et al., 2013; Vrugt et al., 2013; H. Zhang et al., 2017).

A coupled data assimilation (CDA) method is typically employed when the forward model is a coupled system with different types of measurements. CDA is popular due to its ability to enable each model component to receive information from measurements in other domains (S. G. Penny & Hamill, 2017; S. Penny et al., 2019; Laloyaux et al., 2016; Smith et al., 2015; Tardif et al., 2015). In weakly CDA, all model states are predicted simultaneously by a coupled forward model but are updated separately within each domain (S. G. Penny & Hamill, 2017). The updated states are then propagated to the next time step by the coupled model, integrating measurement information from both domains. Conversely, in strongly CDA, states in individual domains are predicted by the coupled model and updated simultaneously using measurements from all domains (Ng et al., 2009). This approach is optimal compared to weakly CDA because it leverages information from all measurements in both the prediction and update steps. However, the successful application of strongly CDA is limited due to the challenges associated with model error covariance (S. Zhang et al., 2020). Defining error covariance in coupled data assimilation is particularly challenging because it requires defining the correlations between states in different domains, which are often the least understood. Although some ensemble data assimilation methods derive correlations through ensemble forecasts, it is difficult to determine if the low-dimensional approximation of the ensemble error covariance is acceptable (Županski, 2017). In methods where the error covariance is not explicitly defined, such as particle filter, the problem still exists because of the low quality of the fundamental Monte Carlo approximation. In addition, particle filter methods introduce issues such as the "Curse of Dimensionality" and particle degeneracy because the state space encompasses all states in both domains in strongly CDA. The drawbacks of strongly CDA were demonstrated in a 5-variable test, where strongly CDA outperformed weakly CDA only when the ensemble size was increased to approximately 10^4 (Han et al., 2013). Consequently, most CDA systems in practical applications are weakly CDA (S. Zhang et al., 2020).

In a synthetic experiment, comparative research on weakly CDA was performed by El Gharamti et al. (2013), where an ensemble Kalman filter was used in a 2D subsurface flow-transport coupled model. The hydraulic head and contaminant concentration observations in multiple wells are assimilated to estimate the evolution of these two states. However, the problem with the Ensemble Kalman Filter (EnKF) persists when the states and observations do not follow a joint multivariate Gaussian distribution.

This study investigates the feasibility of using a weakly coupled particle filtering approach in a landfill TTD model for estimating the emission potential. The emission potential is determined by the waste body's pollutant mass states and water storage states. Based on our knowledge, no research has used particle filtering approaches to estimate both volume quantities and solute concentrations in hydrochemical coupled models. We also believe this is the first time data assimilation has been used to estimate landfill emission potential. Moreover, mass state estimation remains a problem in many data assimilation applications in hydrology. Six synthetic assimilation scenarios were tested to verify the proposed method and optimize the assimilation strategy. Several implementation steps of the algorithm were adjusted to make it suitable for the TTD model. The uncertainties of these hidden states were quantified, and improvement in prediction was evaluated. The chloride mass in the landfill was selected as the representative emission potential in this research.

2. Methods

This data assimilation framework uses a coupled TTD model as the forward model. The weakly coupled particle filter was used as a data assimilation algorithm. The first part of this section describes the theory of weakly coupled particle filter. The second part introduces the forward model and its specific characteristics, which must be addressed in the DA application. The last part concerns synthetic experiment design, implementation procedure, and performance estimation matrices.

2.1. Weakly Coupled Particle Filter

2.1.1. Sequential Importance Sampling

The weakly coupled PF is based on the sequential importance sampling (SIS) PF. Model and measurement equations are required during the state estimation process as given by Arulampalam et al. (2002). We take $\boldsymbol{x}_t$ to represent a state vector that contains all the model states at the current time step t. First, the state vector is propagated from the former time step to the current step with the model equation

$$\boldsymbol{x}_t = M_t(\boldsymbol{x}_{t-1}) + \boldsymbol{\varepsilon}_{model} \quad (1)$$

where $M_t(\cdot)$ denotes the forward model, and $\boldsymbol{\varepsilon}_{model}$ represents the model error vector caused by different sources of uncertainty. The state vector will then be linked to measurements through the measurement equation

$$\boldsymbol{y}_t = H_t(\boldsymbol{x}_t) + \boldsymbol{\varepsilon}_{mea} \quad (2)$$

in which $H_t(\cdot)$ denotes the measurement operator that connects model states to measured states, and $\boldsymbol{\varepsilon}_{mea}$ represents the measurement error vector.

The main task of state estimation is to estimate the probability density function (pdf) of immeasurable states based on measurement series. We use the subscript $1:t$ to represent the time range from the initial step to step t. Hence, $\boldsymbol{y}_{1:t}$ are the available measurements until current step t and $p(\boldsymbol{x}_t|\boldsymbol{y}_{1:t})$ represents the pdf of current state vector $\boldsymbol{x}_t$ given $\boldsymbol{y}_{1:t}$. Bayes' theorem is used to calculate $p(\boldsymbol{x}_t|\boldsymbol{y}_{1:t})$, the so-called posterior pdf, by combining prior pdf $p(\boldsymbol{x}_t|\boldsymbol{y}_{1:t-1})$ from last time step with likelihood pdf $p(\boldsymbol{y}_t|\boldsymbol{x}_t)$ as

$$p(\boldsymbol{x}_t|\boldsymbol{y}_{1:t}) = \frac{p(\boldsymbol{y}_t|\boldsymbol{x}_t)\,p(\boldsymbol{x}_t|\boldsymbol{y}_{1:t-1})}{p(\boldsymbol{y}_t|\boldsymbol{y}_{1:t-1})} \tag{3}$$

$p(\boldsymbol{y}_t|\boldsymbol{y}_{1:t-1})$ is a normalization factor in making sure the integral of pdf is 1. If the posterior pdf $p(\boldsymbol{x}_{t-1}|\boldsymbol{y}_{1:t-1})$ at the previous assimilation step is known, the prior pdf $p(\boldsymbol{x}_t|\boldsymbol{y}_{1:t-1})$ could be calculated as

$$p(\boldsymbol{x}_t|\boldsymbol{y}_{1:t-1}) = \int p(\boldsymbol{x}_t|\boldsymbol{x}_{t-1})\,p(\boldsymbol{x}_{t-1}|\boldsymbol{y}_{1:t-1})\,d\boldsymbol{x}_{t-1} \tag{4}$$

Then we obtain the aim posterior pdf $p(\boldsymbol{x}\,|\,\boldsymbol{y}_{1:t})$ as

$$p(\boldsymbol{x}_t|\boldsymbol{y}_{1:t}) = \frac{p(\boldsymbol{y}_t|\boldsymbol{x}_t)\int p(\boldsymbol{x}_t|\boldsymbol{x}_{t-1})\,p(\boldsymbol{x}_{t-1}|\boldsymbol{y}_{1:t-1})\,d\boldsymbol{x}_{t-1}}{p(\boldsymbol{y}_t|\boldsymbol{y}_{1:t-1})} \tag{5}$$

The core idea of sequential importance sampling is to approximate the required pdf through N independent particles with weight w_i respectively. More specifically, sampling from $p(\boldsymbol{x}_{t-1}|\boldsymbol{y}_{1:t-1})$ means several particles are obtained from the previous time step. $p(\boldsymbol{x}_t|\boldsymbol{x}_{t-1})$ indicates propagating these particles with forward model (Equation 1). The posterior pdf $p(\boldsymbol{x}_t|\boldsymbol{y}_{1:t})$ can be approximated as

$$p(\boldsymbol{x}_t|\boldsymbol{y}_{1:t}) \approx \sum_{i=1}^{N} w_t^i \delta(\boldsymbol{x}_t - \boldsymbol{x}_t^i) \tag{6}$$

In which δ represents the Dirac delta function. N is the number of particles. The w_t^i is calculated recursively as

$$w_t^i = \frac{w_{t-1}^i p(\boldsymbol{y}_t|\boldsymbol{x}_t^i)}{\sum_{i=1}^{N}\left(w_{t-1}^i p(\boldsymbol{y}_t|\boldsymbol{x}_t^i)\right)} \tag{7}$$

The conditional probability $p(\boldsymbol{y}_t|\boldsymbol{x}_t)$ is often computed as a Gaussian likelihood:

$$p(\boldsymbol{y}_t|\boldsymbol{x}_t) = \exp\left\{-0.5\left[\boldsymbol{y}_t - H_t(\boldsymbol{x}_t^i)\right]^T R^{-1}\left[\boldsymbol{y}_t - H_t(\boldsymbol{x}_t^i)\right]\right\} \tag{8}$$

where $H_t(\cdot)$ is the measurement operator, R is the error covariance of the measurements (Van Leeuwen, 2009). Common statistics can be easily acquired with the posterior pdf or weighted particles. For instance, the mean of state vector $\boldsymbol{x}$ is calculated as

$$\bar{\boldsymbol{x}}_t = \sum_{i=1}^{N} w_t^i \boldsymbol{x}^i \tag{9}$$

2.1.2. Systematic Resampling

Particle degeneracy is one main limitation of sequence importance sampling, which occurs after several assimilation steps when the weights of all but one particle can be neglected (Snyder et al., 2008). The effective ensemble size is used to evaluate the degeneracy problem. It is computed as

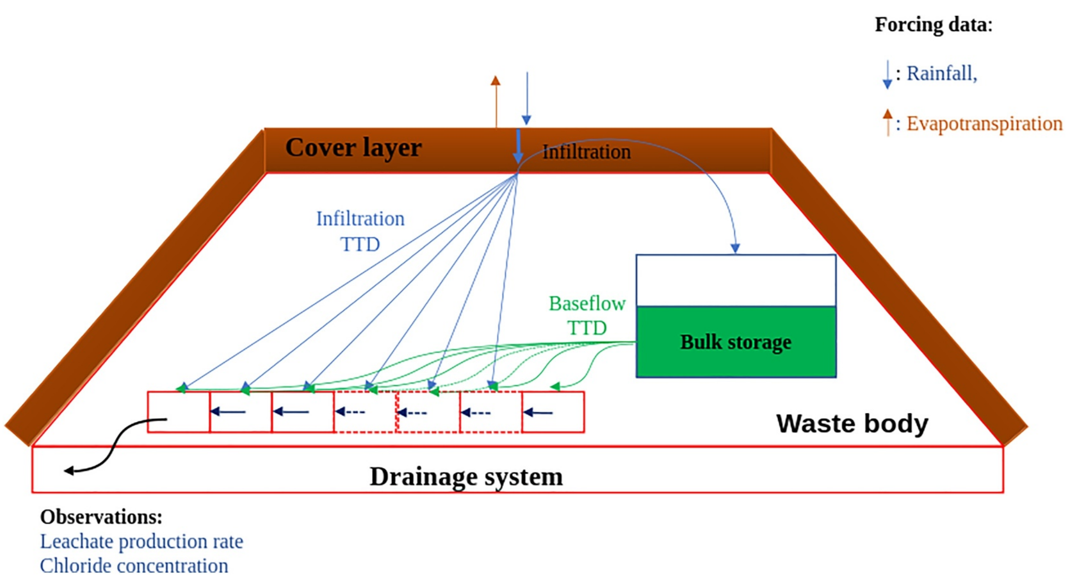

Figure 1. A schematic overview of model structure.

$$N_t^{eff} = \frac{1}{\sum_{i=1}^{N} \left(w_t^i\right)^2} \tag{10}$$

When the effective ensemble size is smaller than $N/2$, resampling should be performed. The idea of resampling is duplicating particles with high weights and discarding those with low weights. After that, all weights will be set as $1/N$. The general resampling algorithms include multinomial, stratified, systematic, and residual resampling methods. In this research, we chose systematic resampling due to its superior resampling quality and computational efficiency compared with the others. A more detailed description of resampling algorithms is given in Hol et al. (2006).

2.1.3. Weakly Coupled Data Assimilation (WCDA)

Coupled data assimilation is used when there is more than one measurement type. Also, a coupled model should be available. In WCDA, a coupled model is used to predict all the model states at the current time step, while the weighting and updating steps are performed within each component domain. Then the updated states are propagated to the next step by the coupled model. Although the measurements in one model domain are used to update the states in the same domain, the coupled model propagates the information to the other domain (S. Zhang et al., 2020). The details about the implementation of WCDA are introduced in Section 2.7.

2.2. Coupled Travel Time Distribution Model

The coupled travel time distribution (TTD) model predicts leachate production rates and chloride concentrations. For a detailed description and implementation of the coupled TTD model, we refer readers to the model paper (Heimovaara & Wang, 2024) and our model scripts (Wang & Heimovaara, 2024). Here, we briefly introduce the model to facilitate understanding of our approach.

As shown in Figure 1, the model consists of two layers representing a cover layer and waste body in a landfill. The forcing data at the top boundary are rainfall (R) and potential evapotranspiration (P_{ev}), which will enter or leave the landfill from the cover layer. The water storage in the cover layer determines the amount of water $\left(q_{\inf}\right)$ infiltrating the waste body. The waste body is conceptually divided into a single bulk storage and P cells to represent different travel times of water parcels before they flow out (discretization of the travel time distribution). The number of mobile cells needs to be large enough to capture the dilution pattern in the travel time distribution of cover layer infiltration but not so large that it assumes the water in the mobile part of the landfill can stay too long. The time difference between neighboring cells is one day. This means that it takes P days for leachate in the

Table 1
Parameters Values and Description in the Coupled TTD Model

Parameter	Values	Description
c_f	9.759×10^{-1}	An empirical crop-factor to compensate for different types of crops in order to close the water balance $[-]$
$\theta_{w_{cl},\max}$	3.437×10^{-1}	Porosity of the cover layer $[-]$
$f_{w_{cl}}, \min$	2.472×10^{-2}	Fraction of the maximum volumetric water content in the cover layer used to describe the minimum water storage in cover layer $[-]$
K_{cl}	-1.960×10^{-1}	The saturated hydraulic conductivity of the cover layer $\left[\mathrm{md}^{-1}\right]$, $10_{\log}$
b_{cl}	5.427	An empirical shape factor for the non-linear flow term of the cover layer $[-]$
τ_{fast}	3.813×10^{1}	Expected value of the fast travel time in the log-normal infiltration travel time distribution $[d]$
σ_{fast}	2.660×10^{-1}	Standard deviation of the travel time in the fast lognormal infiltration travel time distribution [d], $10_{\log}$
$\Delta_{\tau_{slow}}$	7.934×10^{2}	Difference between τ_{fast} and τ_{slow}. $\tau_{slow} = \tau_{fast} + \Delta_{\tau_{slow}}$
σ_{slow}	2.993	Standard deviation of the travel time in the slow lognormal infiltration travel time distribution $[d]$, $10_{\log}$
β_f	6.281×10^{-1}	The fraction of fast flow in the waste body $[-]$
bF_0	-3.368	Maximum value for the baseflow from the bulk storage into the mobile cells. $[m]$, $10_{\log}$
σ_{bF}	-0.294×10^{-1}	Shape factor for the log-normal baseflow function $[m]$, $10_{\log}$.
μ_{bF}	-0.321	Scale parameter of the log-normal baseflow function $[m]$, $10_{\log}$.
κ_{bF}	-8.341	Shape parameter of the baseflow travel time distribution (Gamma distribution) $[m]$.

last cell to exit. It is important to note that these P cells do not refer to physical locations within the waste body, but rather represent leachate parcels with different travel times. The discretization into P cells is a method used to model the distribution of travel times.

The leachate that flows out from bulk storage is considered baseflow, and its volume is a function of bulk water storage. This baseflow is modeled by a log-normal distribution, parameterized by a shape parameter σ_{bF} and a scale parameter $\ln(\mu_{bF})$. The final baseflow value is obtained by multiplying the output of this log-normal distribution and the maximum baseflow value bF_0. The baseflow will then be distributed to P cells according to a Gamma travel time distribution function $\Gamma(\kappa_{bF}, \theta = 1)$. Similarly, the $q_{\inf}$ from the cover layer is distributed to the waste body with another travel time distribution function. The infiltration TTD itself is modeled as a mixture distribution that combines both fast-flow and slow-flow components, each represented by a separate log-normal distribution. We use parameter β_f to describe the fast-flow fraction, and $1 - \beta_f$ is the fraction of slow flow.

Similar to the transport model from El Gharamti et al. (2013), the chloride concentration is one-way coupled in the water balance model. The concentration states in P cells are determined by time propagation, as well as distributed leachate from baseflow and infiltration from the cover layer. The parameters and initial states were optimized using DREAM(ZS) (Shockley, 2020; Vrugt, 2016). The model parameters used in this manuscript is shown in Table 1.

The state vector is given by

$$\boldsymbol{x_t} = [V_{cl_t}, M_{cl_t}, C_{cl_t}, v_{bulk_t}, m_{bulk_t}, c_{bulk_t}, v_{cell_t^i}, m_{cell_t^i}, c_{cell_t^i}]^T \tag{11}$$

where i represents i_{th} cell state. The concentration defined as $c = m/v$ applies to all elements in the conceptual model. Also, $V_{wb_t} = v_{bulk_t} + \sum_{i=0}^{P-1} v_{cell_t^i}$ and $M_{wb_t} = m_{bulk_t} + \sum_{i=0}^{P-1} m_{cell_t^i}$ are used in the following parts to represent the entire storage states in the waste body. C_{wb} indicates the average concentration in the waste body. We use capital letters to represent the overall state variables of each layer, and we use lowercase letters to represent all internal variables. A detailed explanation of the variables in the model is presented in the nomenclature list.

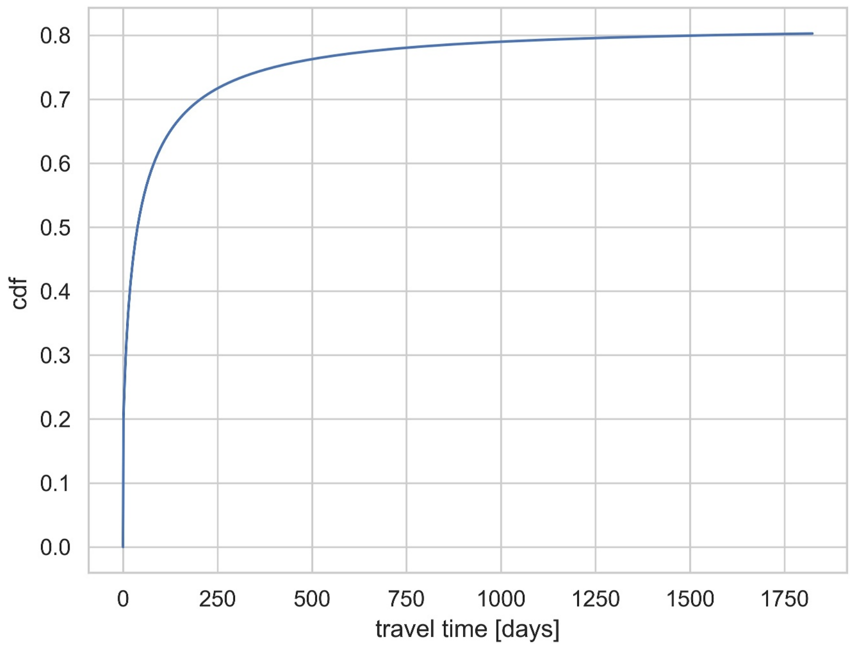

Figure 2. Cumulative distribution of infiltration TTD.

2.3. Specific Model Characteristics

2.3.1. One Way Coupled Model

The TTD model we use is based on a one-way coupling between water volume and chloride concentration. The leachate production rates only contain information on water volume states, while the concentration states depend both on water volume and solute mass. However, it is unknown how much information concentration measurements contain about water volume states. Is it possible to only assimilate concentration measurements, or do we need both the leachate outflow and concentration measurements? El Gharamti et al. (2013) always use the concentration measurements to update the water head states, while the research does not investigate the benefits of assimilating both measurements compared with assimilating only one. Assimilating both measurements could get the best overall estimation for the model states, but it is not necessarily true for specific model parts. For example, when assimilating both types of measurements, the estimation results for volume states may be poorer compared with using only leachate production rate measurements. In order to explore this issue, we have designed different scenarios to investigate the optimal assimilation strategy.

2.3.2. Time Lags in TTD Model

In particle filtering approaches, we can estimate hidden states in the model using measurements of observable states because the measurements contain some information about hidden states. Assuming the model is imperfect, errors will be added to both hidden states and observable states during the state propagation process. One beneficial side effect of introducing model error is that it "rejuvenates" the ensemble of a particle filter. This means that adding model errors to hidden states enables the exploration of the hidden state space more thoroughly. The hidden states with model error will be assessed in the following time steps because they influence the measurable states. However, if this influence is weak or does not exist, the hidden states will be updated randomly, and the estimation will be poor (Plaza Guingla et al., 2013).

In the forward TTD model we use, we have explicit time lags between many model states and measurements because the travel time distribution considers the time information explicitly. At each time step, the model state vector includes thousands of individual cell states as well as a bulk state, which summarizes the entire system. The time lag between the oldest and youngest cell states is determined by the infiltration travel time distribution, with a maximum lag of 5 years, as illustrated in Figure 2. The infiltration water with a travel time larger than 5 years is added to the bulk.

It's important to distinguish between two types of time discretization here: one that tracks the evolution of model states over time and another representing the distribution of travel times for infiltration from a cover layer or baseflow from bulk to exit the system. In this context, a time lag represents the difference in these travel times. As shown in Figure 1, the cells mean the water parcels with different travel times rather than real physical water cells. For instance, the leachate in the oldest cell at time step t will take $P - 1$ days to move to the youngest cell at time step $t + P - 1$. This means the oldest cell will only be reflected in the measurements after P days. This time lag complicates the estimation of multiple hidden states using current measurements.

Several studies are trying to solve these challenges with time-lagged measurements in data assimilation (Li et al., 2013; McMillan et al., 2013; Noh et al., 2013, 2014). McMillan et al. (2013) used the current measurements to update states at previous time steps within the time lag. Noh et al. (2013, 2014) used the measurements after an extended time to estimate current model states to consider the time lag effect. These methods use the forward models as measurement operators to link the model states to corresponding lagged measurements. In these approaches, the assumption is that the forward models are accurate for this extended prediction; otherwise, the representation error (Janjić et al., 2018) in the measurement operator should be considered. The maximum time lag in the landfill TTD model is around 5 years. This is much longer than those previously used in distributed catchment models. Consequently, model error accumulation is expected to be severe during the extended prediction process (Noh et al., 2013, 2014), so it is unreasonable to assume a correct model for such a long prediction period. Additionally, the TTD model has thousands of states that are lagged in time due to the discretization of TTD, whereas the published applications usually have time lag issues for between two states. To overcome these issues, we have developed a specific strategy for the TTD model.

In the TTD landfill model, the cell states are propagated with time. After P (the number of cells) days, there will be a connection among all cells and bulk states. We call this implicit relationship "history." We can estimate hidden states by current measurements if this "history" is maintained. Hence, the initialization of particles and the model errors should guarantee this "history." The implementation strategy is further explained in Section 2.7.

2.4. Site and Data Description

The model parameter calibration is based on actual measurements from the Braambergen landfill in the Netherlands (Duurzaam stortbeheer, 2023). Daily meteorological forcing data (same as model resolution) are obtained from the nearest weather station affiliated with Royal Dutch Meteorological Institute (KNMI) (2023). The leachate is pumped out from the drainage system, and the daily production volume is acquired. The chloride concentration is measured by sampling from the drainage layer generally with a bi-weekly frequency (with some larger intervals up to 28 days). In practical cases, there are many irregular values in daily production rate measurements because of the management of the leachate pump system by the landfill operator. When the pump system is broken, the outflow remains in the drainage layer, resulting in an observed leachate production volume of zero. Afterward, the water is pumped out, a large leachate volume is measured. In order to limit the effect of these operational irregularities, 7 days' average leachate production rates were calculated from the cumulative leachate measurements and used as measurements. The measurement equations for leachate production rate and chloride concentration are:

$$LPR_t = \frac{\sum_{i=t-6}^{t} v_{cell_{0_i}}}{7} + \varepsilon_{LPR_{mea}} \tag{12}$$

$$C_t = c_{cell_{0_t}} + \varepsilon_{C_{mea}} \tag{13}$$

2.5. Synthetic Truth Generation

Synthetic experiments are often designed to evaluate the performance of data assimilation techniques. Artificial truth states are generated by running a known forward model. If the DA algorithm is effective, estimated states or parameters are expected to converge to the synthetic truth by assimilating the simulated measurements obtained from the forward model. The method of creating artificial truth is highly dependent on the aim of the applied DA technique and the assumption of existing underlying uncertainties. The primary sources of uncertainty for a deterministic model are errors in forcing data, initial states, model parameters, and model concepts. The most simple scenario assumes that the model is correct and only adds white noise to simulated measurements as

Table 2
Standard Deviation of Gaussian Random Errors for Truth Generation

Variables	R	Pev	v_{ini}	c_{ini}
Standard deviation	$0.15 \times R_t$	$0.3 \times Pev_t$	$0.1 \times v_{ini}$	$0.1 \times c_{ini}$

Note. v_{ini} and c_{ini} represent all the initial volume and concentration states in the model.

measurement error. Weerts and El Serafy (2006) perturbed forcing data to consider the forcing data uncertainties in a state estimation problem. Plaza Guingla et al. (2013) further added Gaussian noise to model parameters, although only model states are updated in that research. Li et al. (2013) chose to perturb the state variables in a probability-distributed hydrological model. All the uncertainties above are considered to be included in state variables. Gelsinari et al. (2020) used the "truth" generated from the unperturbed model, while the model used in assimilation is with a perturbed parameter set. Since we aim to assess the feasibility of estimating emission potential in the TTD model by coupled particle filter, we assume the forward model parameters to be correct in order to simplify the problem. The initial states and input data were perturbed in order to simulate a scenario where we have a poor understanding of initial states and the input measurements are inaccurate.

The initial states in 2003 were obtained from model calibration in order to generate a synthetic truth. Zero mean Gaussian error with a standard deviation of $10\% \times c_{ini}$ and $10\% \times v_{ini}$ were added to perturb the initial states.

Zero-mean Gaussian errors were added to daily rainfall and potential evapotranspiration during the simulation period from 2003 to 2021. The uncertainty range of rainfall is often chosen as $(0 - 15\%) \times R_t$ (Weerts & El Serafy, 2006). Here the standard deviation of random rainfall error was set as $15\% \times R_t$. The perturbation of evapotranspiration followed Plaza Guingla et al. (2013) where a $30\% \times Pev_t$ standard deviation was used.

Although this study primarily focuses on synthetic experiments, we aim to adapt the framework to accommodate the assimilation of real-world data for further research. Hence, the data assimilation frequency was set to be identical to the frequency of the real concentration measurements.

Once the simulation results are obtained as synthetic truth, the measurement errors should be added to observable states to simulate measurements as shown in Equations 12 and 13. The standard deviations of Gaussian measurement error are selected as 10% of LPR_t and C_t, respectively.

All the errors are presented in Table 2. It is worth emphasizing that although we try to simulate the actual case in the synthetic experiment, the artificial truth is only trying to approach the natural world in the context of a proof-of-concept study (Matgen et al., 2010).

2.6. Ensemble Generation Performance Control

The performance of DA relies on the appropriate representation of uncertainties in the prediction. More specifically, the model error in Equation 1 should make the spread of generated ensembles realistic compared to real measurements. Following the method proposed by De Lannoy et al. (2006), the ensemble spread$(ensp_t)$, the mean square error(mse_t), and the ensemble skill$(ensk_t)$ are calculated as:

$$ensp_t = \frac{1}{N}\sum_{i=1}^{N}\left(y_t^i - \overline{y}_t\right)^2 \tag{14}$$

$$mse_t = \frac{1}{N}\sum_{i=1}^{N}\left(y_t^i - y_{mea_t}\right)^2 \tag{15}$$

$$ensk_t = \left(\overline{y}_t - y_{mea_t}\right)^2 \tag{16}$$

N, i, t, y, y_{mea} represent ensemble size, ith ensemble number, assimilation time step, simulated observable states, and assimilated measurements, respectively. According to De Lannoy et al. (2006), to ensure the generated ensembles' statistical accuracy, the following requirements should be considered:

$$\frac{<ensk>}{<ensp>} \approx 1 \tag{17}$$

<> means the average over the simulation time range. More specifically, a value larger than one indicates insufficient ensemble spread, while a value smaller than one indicates excessive spread. If the truth is indistinguishable from a member of the ensemble, the following equation should be true (De Lannoy et al., 2006):

$$\frac{<\sqrt{ensk}>}{<\sqrt{mse}>} \approx \sqrt{\frac{N+1}{2N}} \tag{18}$$

When both leachate production rate and concentration measurements are assimilated, we need a sufficiently large ensemble spread in the simulated output. This is achieved by manually optimizing the standard deviations of model error. First we obtained the model error for the cover layer water storage using an interval search to get an appropriate spread in leachate production rate simulations. If the spread for concentration states is not sufficient or excessive with the chosen model error, we adjust the initial uncertainty range for the bulk concentration states. Using this approach allows us to obtain a good ensemble spread for concentration states while not making the spread in leachate production excessive.

2.7. Implementation Procedure

Based on the theory and model characteristics, the implementation of sequential importance resampling in this coupled TTD model is as follows:

1. Initialization: from the model calibration results, we take one parameter set and initial states in 2003. The initial samples are sampled from Gaussian distributions where the means are the optimized initial values. Initially, the corresponding percentiles of standard deviations in Gaussian distributions are set to be the same as the ones used in the generation of synthetic initial states (see Table 2). Subsequently, the standard deviations undergo adjustment to meet the ensemble spread criteria, as is discussed in Section 3.1. With a warm-up simulation, the samples are propagated to the starting date of data assimilation on the 19 June 2012, a time step 7 days earlier than the first measurement date. The reason to perform this warm-up propagation is that we need to build connections among waste body states. Otherwise, the time lag between bulk states and measurements will make the estimation unreliable.
2. Update step: all the particles are propagated to the next assimilation step with Equation 1, where $M(\cdot)$ indicates the coupled TTD model. The forward model is discretized with a daily time step, and the assimilation frequency is the same as the real concentration measurement frequency, which is generally 2 weeks. The choice of model error is crucial for representing uncertainties and ensuring a good data assimilation technique performance. Most studies applying particle filter or ensemble Kalman filter choose to add a Gaussian random error to perturb forcing data, model states, and/or parameters (Mattern et al., 2013; Tran et al., 2020; Vrugt et al., 2013; Weerts & El Serafy, 2006). Considering the time lag issue, if we add independent model error to each state directly, the accumulation of errors of states like v_{bulk} will be huge after several years' lag. Therefore, we choose to add daily error to V_{cl}. The daily errors added on day t will be propagated to waste body states since day $t + 1$ according to the infiltration TTD curve with time until the next assimilation step. Therefore, we are actually adding correlated model errors to waste body states. Since the influence of error in V_{cl} on fast flow cells (cells with small travel time) can be estimated by current measurements, we can avoid adding too many unreasonable errors to old states like v_{bulk}. Additionally, this error choice maintains the total mass balance in waste body water storage($V_{wb_{t+1}} = V_{wb_t} + infiltration - outflow$). No model error is introduced to the concentration states directly. Once the initial concentration values are determined, the concentration variation is assumed to be determined by volume states only.
3. Analysis step: The particle weights are calculated by Equation 7. Based on different assimilation strategies, we weigh the states differently. In a coupled assimilation scenario, the weights for volume w_v and concentration states w_c are calculated separately using their corresponding measurements. Both concentration and leachate volume are used to calculate w_m: $w_m = w_c * w_v$. Then w_m is normalized before estimating the mass states. If only concentration measurements are assimilated, all the model states are weighted based on the concentration measurements. When only LPR measurements are assimilated, the weights are used to estimate all states except concentration states.
4. Resampling step: this step is similar to the analysis step, effective ensemble size N_v^{eff}, N_c^{eff} is computed according to Equation 10. Then the volume states will be resampled when N_v^{eff} is smaller than $N/2$. The concentration states will be resampled if N_c^{eff} is smaller than $N/2$. These two resampling steps are totally

Table 3
Synthetic Scenarios

Scenario	Assimilate LPR	Assimilate C	Small initial V_{bulk}
A	Yes	Yes	No
B	Yes	No	No
C	No	Yes	No
D	Yes	Yes	Yes
E	Yes	No	Yes
F	No	Yes	Yes
$OL_{A\text{-}C}$	No	No	No
$OL_{D\text{-}F}$	No	No	Yes

separated, which means the resampling of volume states will not change the concentration states and their weights w_c, and vice versa. If volume or concentration states are resampled, the mass states will be recalculated based on the current volume and concentration states, and the weights w_m are also updated with new w_v and w_c. The resampled volume and concentration states are then used in the coupled forward model to make a prediction until the next assimilation step.

5. Iteration: all former steps after initialization are repeated until the last assimilation step.

2.8. Performance Estimation

Besides the evolution of hidden states, the accuracy of state estimation results is evaluated with the temporal mean root-mean-square error, which is described in Equation 19. The L indicates the number of assimilation time steps.

$$MRMSE = \frac{\sum_{t=1}^{L} \sqrt{\sum_{i=1}^{N} w_t^i \left(x_t^i - x_t^{truth}\right)^2}}{L} \tag{19}$$

The prediction accuracy is also evaluated using a logarithmic form(η) proposed by Ercolani and Castelli (2017):

$$\eta = -\ln(1 - NSE) \tag{20}$$

Where NSE is the Nash-Sutcliffe efficiency calculated as:

$$NSE = 1 - \frac{\sum_{t=1}^{T} \left(y_t - y_{mea_t}\right)^2}{\sum_{t=1}^{T} \left(y_{mea_t} - \overline{y_{mea}}\right)^2} \tag{21}$$

where y_{mea_t} are the measurements at time step t, y_t represents the model prediction, and the over bar means the average over time. The logarithmic scale allows dealing with high NSE values (close to 1). It tends to plus infinity when the observations and predictions achieve a perfect match. The reliability of ensemble prediction is not considered here because the model error is optimized to get reliable predictions.

2.9. Synthetic Scenarios

Different synthetic scenarios are designed to test the application's feasibility. As shown in Table 3, in total six scenarios are used to test the assimilation performance and get optimal assimilation strategy. Scenarios A, D follow the proposed coupled assimilation procedure described above. In other scenarios, only LPR or concentration measurements are assimilated. The concentration observations are used to estimate all states when assimilated solely, while the LPR observations are used to update volume states solely. This is because concentration measurements contain information on both volume and concentration states, while the LPR observations only contain information on volume states. Scenarios D to F are similar to A to C but with the difference that we initialize the simulation with much smaller initial bulk volume values. These scenarios are used to test the influence of the baseflow function, which will be discussed in the following part. Two open-loop simulations are also performed to get reference results for scenarios $A - C$ and $D - E$. The open loop simulations have the same initial sample distributions and model errors as corresponding scenarios, but no measurements are assimilated to update model states.

3. Results and Discussion

The results of the experiment will be presented as follows. First, we present the performance of ensemble generation. Next, we discuss the hidden state estimations, including cover layer water storage, total water storage, average concentration, and total chloride mass in the waste body. Finally, we show the prediction performance results across all scenarios. Based on our experimental scenario settings, we will primarily make two types of

10.1029/2023WR036549

Table 4
Ensemble Generation Performance

Scenario	$M_{v_{bulk}}$	$\sigma_{v_{bulk}}$	$\sigma_{c_{bulk}}$	$\epsilon_{V_{cl}}$	$\frac{<ensk>}{<ensp>}_{LPR}$	$\frac{<\sqrt{ensk}>}{<\sqrt{mse}>}_{LPR}$	$\frac{<ensk>}{<ensp>}_{C}$	$\frac{<\sqrt{ensk}>}{<\sqrt{mse}>}_{C}$
A-C	4.067	0.100	0.130	0.0145	1.002	0.651	1.082	0.587
D-E	2.000	0.100	0.100	0.0135	0.998	0.624	1.013	0.583

Note. All the initial states in 2003 are sampled from Gaussian distributions $N(M, \sigma \times M)$. The distribution parameters are the same as truth generation if not explicitly defined in the table. $M_{v_{bulk}}$ represents the initial mean of bulk water storage. $\sigma_{v_{bulk}}$ and $\sigma_{c_{bulk}}$ refer to the standard deviation percentile of bulk water storage and chloride concentration, respectively. $\epsilon_{V_{cl}}$ shows the standard deviation percentile for Gaussian model error ($N(0, \epsilon_{V_{cl}} \times V_{cl})$) added to cover layer water storage. If the newly generated cover layer water storage with model error is negative, we manually set it to a small value of 0.001.

comparisons: one between scenarios with different initial bulk storage states, and another between scenarios with the same initial bulk storage but different measurements assimilated.

3.1. Ensemble Generation

The appropriateness of ensemble generation and the generated initial particles on the starting date of data assimilation, which is the 19th of June, is verified using Equations 17 and 18. Based on the results of a preliminary sensitivity analysis of ensemble size, all experiments use 10,240 particles to ensure stable performance. The final choice of initialization, model errors and the corresponding ensemble generation skills are presented in Table 4.

3.2. Assimilation Performance

3.2.1. Estimation of Hidden States

The hidden state estimation performance of the method is evaluated using the proposed performance matrices (Equations 19–21). The results of total water storage in the cover layer, chloride mass, and water storage in the waste body are presented in Figure 3. In addition, the results of average chloride concentration are presented to understand the state update process better. Although there is a small amount of chloride in the cover layer, it can be ignored compared with the amount in the waste body.

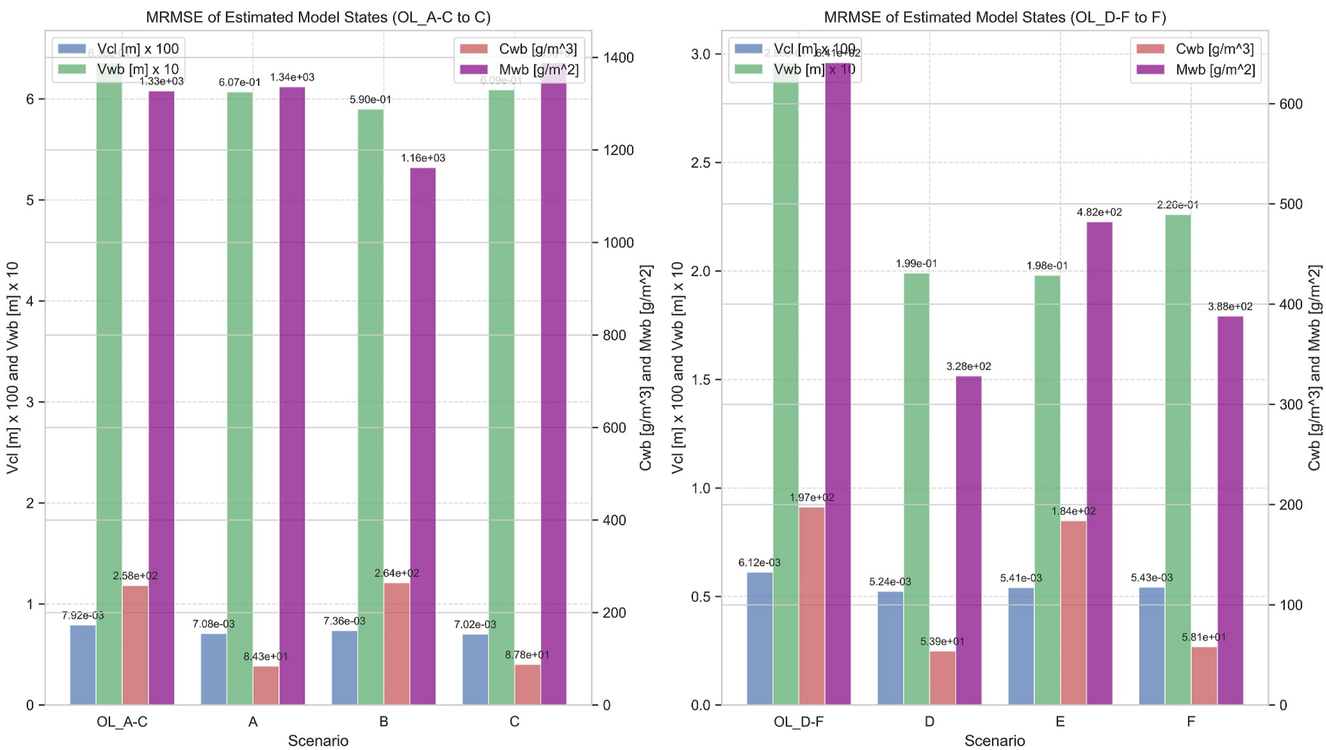

Figure 3. MRMSE of hidden states in different scenarios.

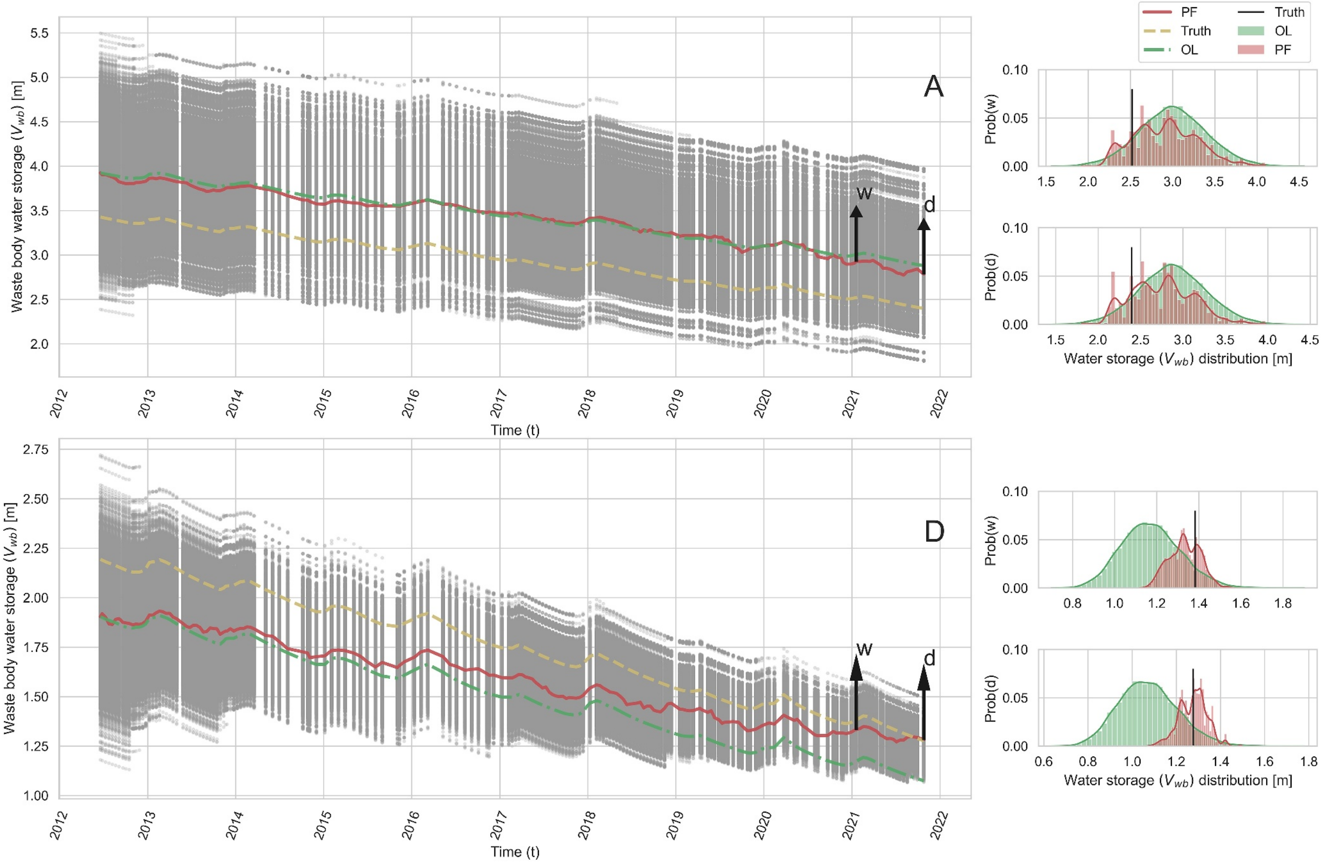

Figure 4. Water storage in the waste body in scenarios A and D. The red line represents the mean estimation of the particle filter. The green and yellow lines represent the open loop results and synthetic truth, respectively. The individual particles are shown as gray points. The two black arrows point to the wet and dry period during the assimilation process, with corresponding probabilities plotted. The black vertical lines in the probability histograms are the truth at specific time steps.

3.2.1.1. Total Water Storage in Cover Layer

As shown in Figure 3, the four MRMSE values for the storage in the cover layer (V_{cl}) in A-C and OL_{A-C} scenarios are similar. This observation is supported by the standard deviations of MRMSE, which are within a magnitude of 4×10^{-3}m. Similar estimation performance is observed in scenarios D-F and OL_{D-F}, where the standard deviations of MRMSE are within a magnitude of 3×10^{-3}m. The values of the standard deviations of RMSE are in the uploaded output file. The similar behavior of cover layer water storage is mainly caused by the buffering effect of the unsaturated soil model used to simulate V_{cl}. When saturation is high, infiltration to the waste body will be high as well. If no model error or forcing data errors were added, the V_{cl} starting with different values would converge to a same value after a period of time. The random model error added during data assimilation is the main source of the uncertainty in V_{cl}.

3.2.1.2. Total Water Storage in Waste Body

Scenarios A–C are initialized with high values for initial bulk water storage. As shown in Figure 3, scenario B has similar waste body water storage (V_{wb}) estimation results as scenario A because of the same assimilation procedure for volume states.

As shown in Figure 4, the mean estimation shows no noticeable improvement throughout the entire period in scenario A. However, when the model is initialized with a lower value for the initial bulk water storage in scenario D, the behavior differs significantly. The assimilation of new measurements corrects the biases in total water storage compared to the scenarios with large bulk water storage. Scenarios D and E also exhibit better estimation performance than open-loop simulations, unlike scenarios B and C, where only slight improvement is observed, as illustrated in Figure 3.

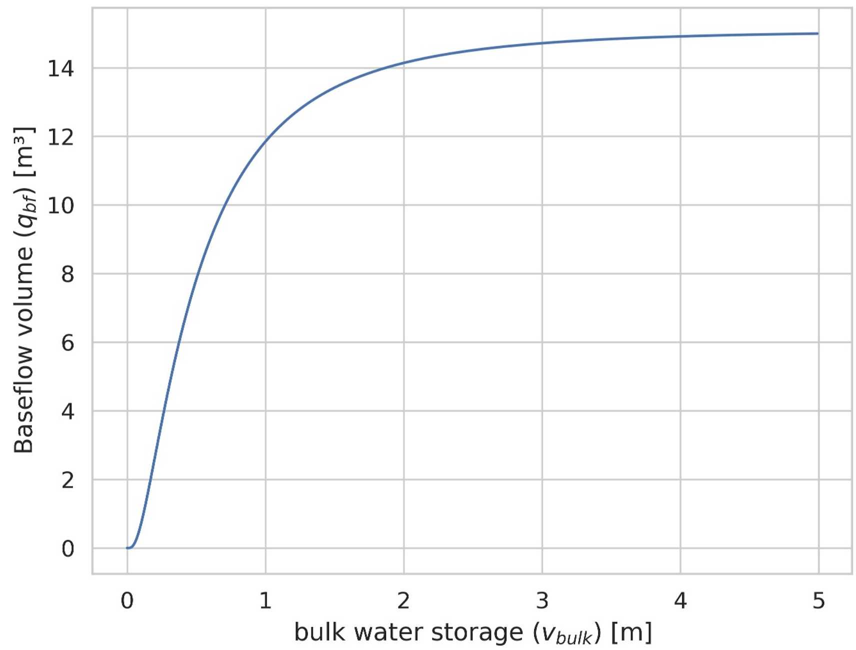

Figure 5. Baseflow change with bulk water storage variation.

The difference in assimilation performance between the two initial values in water storage is due to the baseflow function. As discussed regarding the time lag issue, we can only estimate hidden states if the measurements are sensitive to their variations. Figure 5 shows the baseflow function, which links bulk water storage to the generated baseflow volume. Bulk water storage constitutes a significant portion of the total water storage in the waste body, making its estimation crucial for accurate V_{wb} estimation. As shown, baseflow is sensitive to variations in bulk water storage only when it ranges between 0 and 2 m. Additionally, Figure 6 illustrates the travel time distribution of baseflow, indicating that almost all generated baseflow is allocated to the oldest cell. This means any changes in bulk storage take 5 years to be reflected in simulated leachate production rates.

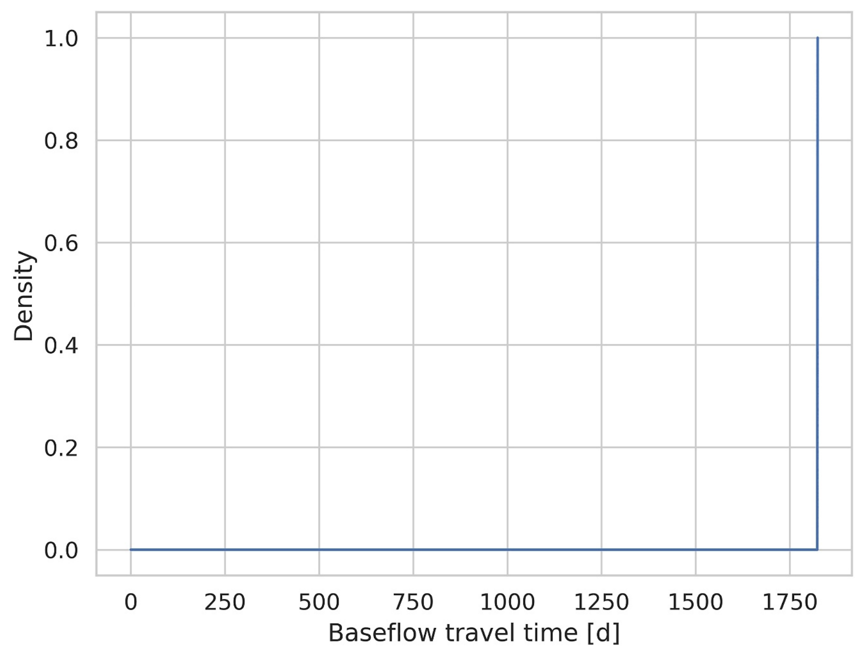

Figure 6. Baseflow travel time distribution.

According to the synthetic truth, the bulk water storage 5 years before the last measurement in scenarios A-C is around 2.18 m. Obviously, the information in the measurements to quantify bulk water storage is limited. Lower values of the bulk water storage allow the baseflow to reduce during the simulation time span. As a consequence, measured leachate production rates contain information on this reduced water storage because of lower baseflow values. This improves the estimate of bulk water storage and V_{wb}, leading to lower uncertainty. It's worth noting that selecting different baseflow functions or baseflow distribution functions from the MCMC results can lead to varying state estimation outcomes. This paper aims to investigate the feasibility of using the coupled particle filter method in a synthetic experiment, assuming our model parameters are accurate. Additionally, we will explore the influence of parameter uncertainty in subsequent research.

Another influencing factor of the uncertainty quantification capacity is the measurement error. While the measurement errors are small, it can detect smaller baseflow changes. For example, the bulk water content will still influence the baseflow when it varies between 2 and 3 m. When the measurement error is relatively large compared to the corresponding baseflow variation, most of the particle sets in this range will have close weights as they all give similar baseflow output. As shown in scenario A in Figure 4, only large and small particle sets are discarded with assimilation.

In scenario A, the posterior distribution in wet periods is close to the ones obtained during dry periods. This means that the estimation results of V_{wb} are stable during the last wet-dry cycle. However, in scenario D, the posterior distributions in dry periods still change compared with wet periods. This indicates that the measurements in the last cycle still contain new information content which are being assimilated to reduce the uncertainty. To further quantify the uncertainty and correct the bias in mean estimation, the time series of measured leachate production rates should be long enough to capture the effect of reducing bulk water storage values in the sensitive range.

Comparing scenarios assimilating different measurements, Figure 3 shows that when the information content of the measurements is high, the concentration measurements can be used to estimate V_{wb} in scenario F. Compared with scenario D, the MRMSE in scenario F is higher. It is because the weights in scenario F are calculated using concentration measurements, which are also influenced by mass states. The particles with the wrong volume and mass values but correct concentration values are also considered with high probability.

3.2.1.3. Average Chloride Concentration in Waste Body

Estimation of the average chloride concentration in the waste body is another case where the “history” is required. All available measurements are linked to the first cell only. Nevertheless, the estimation of the average concentration becomes possible because of the “history” connection between cells and bulk.

As shown in Figure 3, the MRMSE values in average concentration are lower when concentration measurements are assimilated, compared with the open-loop results. As shown in Figure 7, in both scenarios A and D, the uncertainties are significantly reduced, and the synthetic truth is covered by the particles. Regardless of the sensitivity of baseflow to variations in bulk water storage, the chloride in the waste body bulk serves as the source for chloride in the mobile cells, enabling us to use concentration measurements to estimate the average concentration effectively.

It is worth noting that when only concentration states are assimilated in scenarios B and F, Figure 3 shows slightly higher MRMSE values compared with scenarios A and D, where both concentration and LPR measurements are assimilated. Similarly, the MRMSE of average concentration in scenario E is slightly better than the open-loop group. This indicates that the assimilation of LPR measurements helps improve the estimation of concentration states. Although concentration states are updated solely by concentration measurements, the updated volume states influence the prediction of concentration states at the next time step. This illustrates how weakly coupled data assimilation integrates information from both domains. We did not observe this behavior in waste body water storage estimation because our model is one-way coupled. This effect is likely not very strong, probably because our initial particles for volume states can generate good volume predictions due to optimization by MCMC. Overall, the assimilation of concentration states helps quantify the uncertainty in concentration states.

3.2.1.4. Total Chloride Mass in Waste Body

The total chloride mass in the waste body is calculated from the estimated water volume and concentration states. The uncertainty reduction in either volume states or concentration states reduces the uncertainty of mass states.

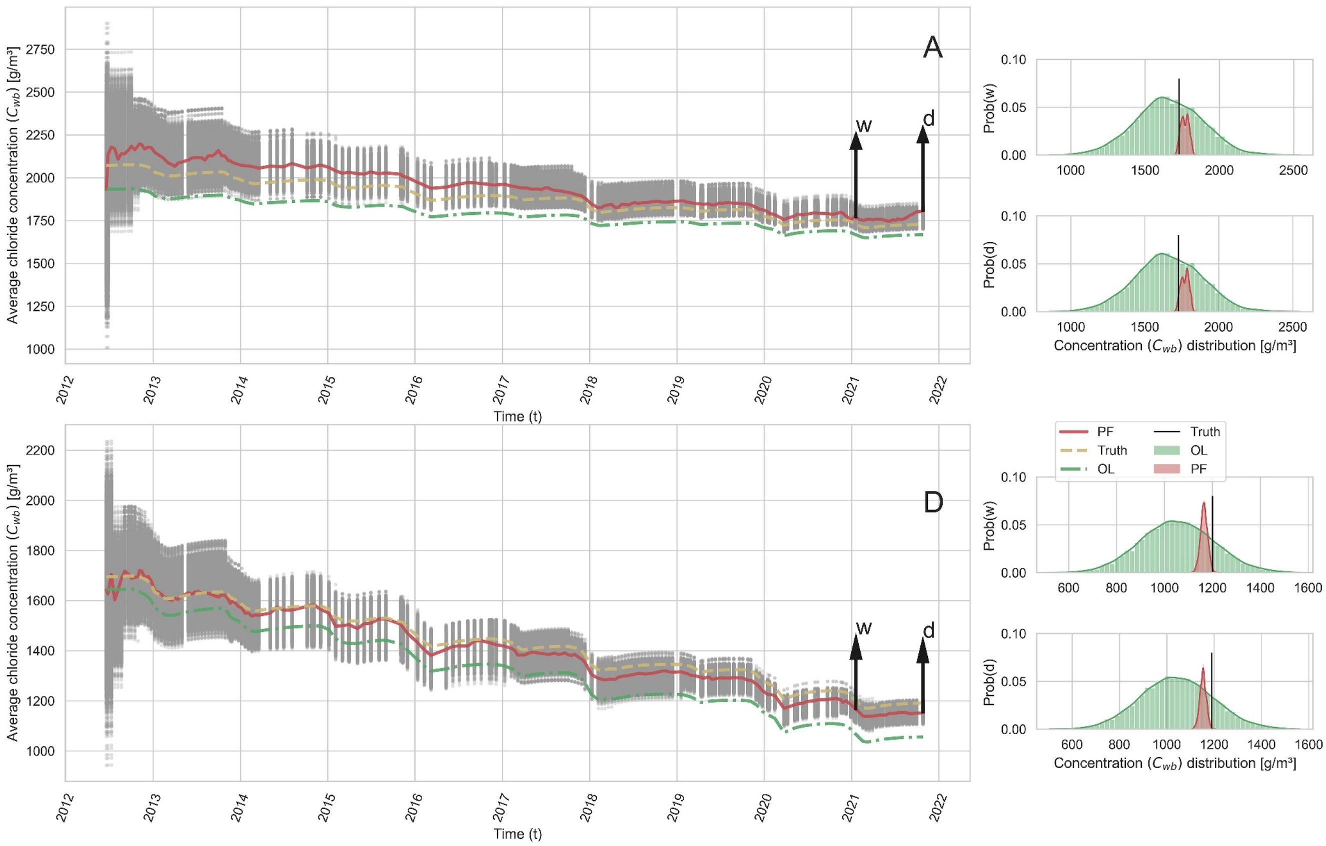

Figure 7. Average concentration in the waste body in scenarios A and D. Colors of lines as in Figure 3.

On the other hand, bias in the estimation of volume or concentration states can result in bias in mass estimation, even if the other estimation is perfect.

As shown in Figure 3, when initial bulk water storage is small, all the synthetic experiments have better MRMSE results than open-loop simulations. Assimilating both measurements achieves the best estimation results. In contrast, when the initial bulk storage is high, the MRMSE decrease is relatively small after assimilation. This is because the uncertainty in V_{wb} is not sufficiently reduced in scenarios A, B, and C. Scenario B's MRMSE result is unusually small because it yields a higher estimation of water storage and a lower estimation of average concentration states, leading to a better mean estimation of mass states.

Following the conclusion from volume and concentration estimations, solely assimilating LPR measurements is insufficient for emission potential estimation. When the sensitivity of baseflow to bulk storage is high, we can use concentration measurements solely to estimate the M_{wb}. Assimilating both measurements achieves the best performance in the sense of both mean estimation and uncertainty reduction.

3.2.2. Prediction Performance

3.2.2.1. Leachate Production Rates

Figure 8 shows the metrics we use to quantify the quality of the predicted states. All six scenarios have smaller MRMSE values and greater η values compared with the corresponding open-loop simulations. This indicates reduced prediction uncertainty and improved accuracy. However, the η and NSE values of three scenarios with the same initial bulk storage are very close.

As discussed in Section 3.2.1.1, the estimation of cover layer water storage has a relatively good consistency with the truth because of the buffering effect, which guarantees the accuracy of LPR prediction, especially in wet periods where infiltration from the cover layer takes up most of the outflow. Additionally, when the bulk storage

10.1029/2023WR036549

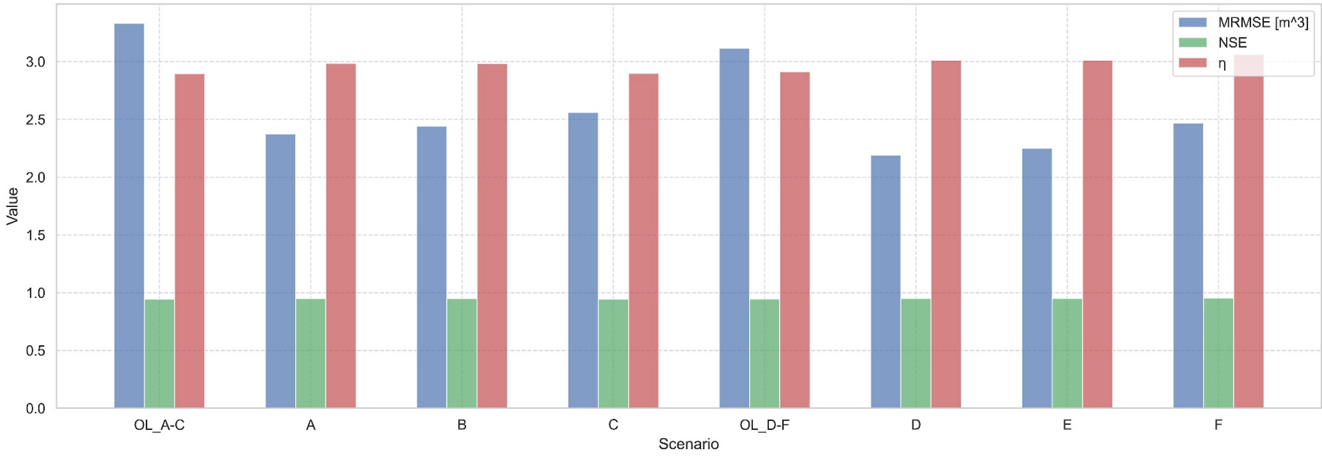

Figure 8. LPR prediction performance in different scenarios.

in the waste body, v_{bulk}, reduces below 1 m (see Figure 5), the baseflow magnitude will reduce significantly. Under such conditions, baseflow will show a large sensitivity to infiltration from the cover layer reaching the bulk storage.

Although scenario D, as shown in Figure 3, provides a better estimation of waste body water storage than scenario F, scenario F has a higher η value compared to scenario D. This is likely because more uncertainty remained in the posterior distribution of scenario F, which is crucial for capturing the effect of changes in bulk storage on the baseflow. Additionally, η is calculated using synthetic measurements that include measurement errors. During the dry period, some values are smaller than the true values, which can only be accounted for by small v_{bulk} values.

3.2.2.2. Chloride Concentrations

As shown in Figure 9, when concentration measurements are assimilated in scenarios A, C, D, and F, the values of prediction accuracy η improve significantly compared with open-loop realizations. When only LPR measurements are assimilated, we also observe the reduction of MRMSE and improvement of η. Although the improvement is very small compared with the scenarios assimilating concentrations, it shows the improvement in flow estimation can help improve the concentration prediction.

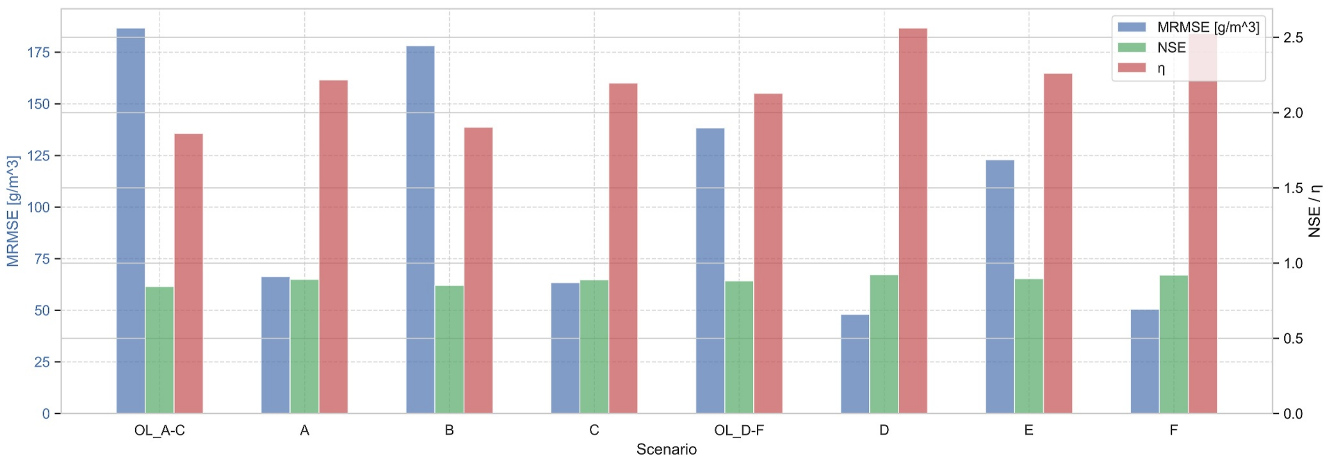

Figure 9. Concentration prediction performance in different scenarios.

4. Summary and Conclusions

This work presents a weakly coupled particle filter framework to assimilate leachate production rates and chloride concentrations with the aim of estimating the emission potential of landfill waste bodies. The emission potential in this paper is defined as the mass of leachable chloride present in the waste body. A concentration-coupled travel time distribution model was used as a forward model for data assimilation. Synthetic experiments were performed to investigate the feasibility of state estimation and improving prediction. Six scenarios were developed to investigate the best assimilation strategy. Two synthetic measurement data sets were generated with the same forward model using different initial bulk water content values under identical meteorological forcing conditions. On each synthetic data set, three types of Data Assimilation were carried out: DA using both Leachate Production Rate (LPR) and concentration measurements and DA using only LPR or concentration measurements.

The results from the different scenarios show that the sensitivity of baseflow to bulk water storage volume plays a vital role in controlling the assimilation performance. When the bulk water storage is within the range where its change has limited influence on baseflow, assimilating measurements cannot reduce the uncertainties in waste body water storage. This indicates that we need to record measurements over a long enough period to capture the sensitive range. Additionally, proactive measures should be implemented to stimulate the emission of bulk water storage, allowing us to reach the sensitive range more quickly.

The results also indicate that the improvement in the estimation of cover layer water storage is limited as the open-loop realizations already have good consistency with synthetic truth. Assimilating concentration measurements improves the estimation of average concentration states in the waste body. It also benefits the estimation of water storage states as the concentration states are coupled to the water balance model. However, assimilation with concentration measurements alone behaves worse in water storage estimation in comparison with assimilating both LPR and concentration measurements under the assumed measurement errors in this research. In contrast, assimilating LPR helps quantify the uncertainty in water storage states in the waste body, while it doesn't reduce the uncertainties in concentration states. The proposed coupled assimilation method leads to good estimation results in both water storage and concentration states. More specifically, better concentration estimation performance is observed in coupled assimilation compared with assimilating concentration solely, which indicates the benefit of information exchange in forecast steps.

The estimation of emission potential heavily relies on accurate estimation of the total water storage and concentration states within the waste body. Reducing uncertainties in volume or concentration states leads to a corresponding reduction in uncertainties associated with emission potential. Therefore, improving the estimation of volume and concentration states directly contributes to minimizing uncertainties in emission potential. The results show the uncertainty is reduced in all the tested scenarios where the baseflow is sensitive to bulk storage change. The LPR prediction improvement after assimilation is insignificant, as the open-loop realizations also have good predictions. In contrast, the concentration predictions improved considerably when the chloride concentration measurements were assimilated.

Overall, the results of this study indicate that the proposed coupled assimilation procedure can be used to estimate total water storage and chloride mass in the waste body. As such, Data Assimilation is demonstrated to be a viable approach for quantifying the emission potential of landfill waste bodies. The assimilation of LPR rates helped improve the accuracy of the estimation of total water storage, V_{wb}, compared to assimilating concentrations alone. The gap between volume states and mass states is filled by concentration assimilation. Although the coupled assimilation was performed at the same time steps, this method can easily be expanded to assimilate different types of measurements at different time steps. This synthetic experiment assumes a perfect model so that the time lag issue can be solved by adding daily model errors to cover layer states. In a real case study, we must combine the state and parameter estimation to account for the parameter uncertainty. We may also need to independently add model errors to all states if we consider the model conceptual error. Extra measurements, such as hydrogeophysical observations for the whole waste body, may be required to further quantify the uncertainty without suffering the time lag problem. Future studies will focus on quantifying the uncertainty caused by model parameters, which, for example, determine the sensitivity of baseflow to bulk water storage volume.

Data Availability Statement

All data and scripts used in this paper are available at (Wang & Heimovaara, 2024).

Acknowledgments
This research is part of the CURE project supported by the Dutch National Science Foundation (NWO) under project no. OCENW.GROOT.2O19.O92. The research is also supported by the Dutch Sustainable Landfill Foundation via the iDS project. The authors also express appreciation to the support from Chinese Scholarship Council (No. 201906090271).

References

Abbaszadeh, P., Moradkhani, H., & Daescu, D. N. (2019). The quest for model uncertainty quantification: A hybrid ensemble and variational data assimilation framework. *Water Resources Research*, *55*(3), 2407–2431. https://doi.org/10.1029/2018WR023629

Arulampalam, M. S., Maskell, S., Gordon, N., & Clapp, T. (2002). A tutorial on particle filters for online nonlinear/non-Gaussian Bayesian tracking. *IEEE Transactions on Signal Processing*, *50*(2), 174–188. https://doi.org/10.1109/78.978374

Brand, E. (2014). *Development of emission testing values to assess sustainable landfill management on pilot landfills: Phase 2: Proposals for testing values*. Rijksinstituut voor Volksgezondheid en Milieu RIVM.

Carrassi, A., Bocquet, M., Bertino, L., & Evensen, G. (2018). Data assimilation in the geosciences: An overview of methods, issues, and perspectives. *Wiley Interdisciplinary Reviews: Climate Change*, *9*(5), e535. https://doi.org/10.1002/wcc.535

De Lannoy, G. J., Houser, P. R., Pauwels, V. R., & Verhoest, N. E. (2006). Assessment of model uncertainty for soil moisture through ensemble verification. *Journal of Geophysical Research*, *111*(D10). https://doi.org/10.1029/2005JD006367

Djurić, P., Kotecha, J., Zhang, J., Huang, Y., Bugallo, M., & Miguez, J. (2003). Particle filtering. *IEEE Signal Processing Magazine*, *20*(5), 19–38. https://doi.org/10.1109/msp.2003.1236770

Duurzaam stortbeheer. (2023). English page. Retrieved from https://duurzaamstortbeheer.nl/english-page/

El Gharamti, M., Hoteit, I., & Valstar, J. (2013). Dual states estimation of a subsurface flow-transport coupled model using ensemble Kalman filtering. *Advances in Water Resources*, *60*, 75–88. https://doi.org/10.1016/j.advwatres.2013.07.011

Ercolani, G., & Castelli, F. (2017). Variational assimilation of streamflow data in distributed flood forecasting. *Water Resources Research*, *53*(1), 158–183. https://doi.org/10.1002/2016WR019208.Received

Evensen, G. (2003). The ensemble Kalman filter: Theoretical formulation and practical implementation. *Ocean Dynamics*, *53*(4), 343–367. https://doi.org/10.1007/s10236-003-0036-9

Fatoba, J. O., Eluwole, A. B., Sanuade, O. A., Hammed, O. S., Igboama, W. N., & Amosun, J. O. (2021). Geophysical and geochemical assessments of the environmental impact of abule-egba landfill, southwestern Nigeria. *Modeling Earth Systems and Environment*, *7*(2), 695–701. https://doi.org/10.1007/s40808-020-00991-8

Fellner, J., & Brunner, P. H. (2010). Modeling of leachate generation from MSW landfills by a 2-dimensional 2-domain approach. *Waste Management*, *30*(11), 2084–2095. https://doi.org/10.1016/j.wasman.2010.03.020

Fellner, J., Döberl, G., Allgaier, G., & Brunner, P. H. (2009). Comparing field investigations with laboratory models to predict landfill leachate emissions. *Waste Management*, *29*(6), 1844–1851. https://doi.org/10.1016/j.wasman.2008.12.022

Gelsinari, S., Doble, R., Daly, E., & Pauwels, V. R. (2020). Feasibility of improving groundwater modeling by assimilating evapotranspiration rates. *Water Resources Research*, *56*(2), e2019WR025983. https://doi.org/10.1029/2019WR025983

Grugnaletti, M., Pantini, S., Verginelli, I., & Lombardi, F. (2016). An easy-to-use tool for the evaluation of leachate production at landfill sites. *Waste Management*, *55*, 204–219. https://doi.org/10.1016/j.wasman.2016.03.030

Gworek, B., Dmuchowski, W., Koda, E., Marecka, M., Baczewska, A. H., Bragoszewska, P., et al. (2016). Impact of the municipal solid waste łubna landfill on environmental pollution by heavy metals. *Water*, *8*(10), 470. https://doi.org/10.3390/w8100470

Han, G., Wu, X., Zhang, S., Liu, Z., & Li, W. (2013). Error covariance estimation for coupled data assimilation using a Lorenz atmosphere and a simple pycnocline ocean model. *Journal of Climate*, *26*(24), 10218–10231. https://doi.org/10.1175/JCLI-D-13-00236.1

Heimovaara, T. J., & Wang, L. (2024). Quantification of emission potential of landfill waste bodies using a stochastic leaching framework. *Authorea Preprints*. https://doi.org/10.22541/essoar.172072859.94113940/v1

Hol, J. D., Schon, T. B., & Gustafsson, F. (2006). On resampling algorithms for particle filters. In *2006 IEEE nonlinear statistical signal processing workshop* (pp. 79–82). https://doi.org/10.1109/NSSPW.2006.4378824

Janjić, T., Bormann, N., Bocquet, M., Carton, J., Cohn, S. E., Dance, S. L., et al. (2018). On the representation error in data assimilation. *Quarterly Journal of the Royal Meteorological Society*, *144*(713), 1257–1278. https://doi.org/10.1002/qj.3130

Kattenberg, W., & Heimovaara, T. (2011). Policy process of allowing research pilots for sustainable emission reduction at landfills in The Netherlands. In *Proceedings Sardinia*.

Laloyaux, P., Balmaseda, M., Dee, D., Mogensen, K., & Janssen, P. (2016). A coupled data assimilation system for climate reanalysis. *Quarterly Journal of the Royal Meteorological Society*, *142*(694), 65–78. https://doi.org/10.1002/qj.2629

Laner, D., Fellner, J., & Brunner, P. H. (2011). Future landfill emissions and the effect of final cover installation–a case study. *Waste Management*, *31*(7), 1522–1531. https://doi.org/10.1016/j.wasman.2011.02.022

Li, Y., Ryu, D., Western, A. W., & Wang, Q. (2013). Assimilation of stream discharge for flood forecasting: The benefits of accounting for routing time lags. *Water Resources Research*, *49*(4), 1887–1900. https://doi.org/10.1002/wrcr.20169

Liu, Y., & Gupta, H. V. (2007). Uncertainty in hydrologic modeling: Toward an integrated data assimilation framework. *Water Resources Research*, *43*(7). https://doi.org/10.1029/2006WR005756

Liu, Y., Weerts, A., Clark, M., Hendricks Franssen, H.-J., Kumar, S., Moradkhani, H., et al. (2012). Advancing data assimilation in operational hydrologic forecasting: Progresses, challenges, and emerging opportunities. *Hydrology and Earth System Sciences*, *16*(10), 3863–3887. https://doi.org/10.5194/hess-16-3863-2012

Matgen, P., Montanari, M., Hostache, R., Pfister, L., Hoffmann, L., Plaza, D., et al. (2010). Towards the sequential assimilation of SAR-derived water stages into hydraulic models using the particle filter: Proof of concept. *Hydrology and Earth System Sciences*, *14*(9), 1773–1785. https://doi.org/10.5194/hess-14-1773-2010

Mattern, J. P., Dowd, M., & Fennel, K. (2013). Particle filter-based data assimilation for a three-dimensional biological ocean model and satellite observations. *Journal of Geophysical Research: Oceans*, *118*(5), 2746–2760. https://doi.org/10.1002/jgrc.20213

McMillan, H., Hreinsson, E., Clark, M., Singh, S., Zammit, C., & Uddstrom, M. (2013). Operational hydrological data assimilation with the recursive ensemble Kalman filter. *Hydrology and Earth System Sciences*, *17*(1), 21–38. https://doi.org/10.5194/hess-17-21-2013

Ng, G.-H. C., McLaughlin, D., Entekhabi, D., & Scanlon, B. (2009). Using data assimilation to identify diffuse recharge mechanisms from chemical and physical data in the unsaturated zone. *Water Resources Research*, *45*(9). https://doi.org/10.1029/2009WR007831

Noh, S. J., Rakovec, O., Weerts, A. H., & Tachikawa, Y. (2014). On noise specification in data assimilation schemes for improved flood forecasting using distributed hydrological models. *Journal of Hydrology*, *519*, 2707–2721. https://doi.org/10.1016/j.jhydrol.2014.07.049

Noh, S. J., Tachikawa, Y., Shiiba, M., & Kim, S. (2013). Ensemble Kalman filtering and particle filtering in a lag-time window for short-term streamflow forecasting with a distributed hydrologic model. *Journal of Hydrologic Engineering*, *18*(12), 1684–1696. https://doi.org/10.1016/j.jhydrol.2014.07.049

Pantini, S., Verginelli, I., & Lombardi, F. (2014). A new screening model for leachate production assessment at landfill sites. *International journal of Environmental Science and Technology*, *11*(6), 1503–1516. https://doi.org/10.1007/s13762-013-0344-7

Penny, S., Bach, E., Bhargava, K., Chang, C.-C., Da, C., Sun, L., & Yoshida, T. (2019). Strongly coupled data assimilation in multiscale media: Experiments using a quasi-geostrophic coupled model. *Journal of Advances in Modeling Earth Systems*, *11*(6), 1803–1829. https://doi.org/10.1029/2019MS001652

Penny, S. G., & Hamill, T. M. (2017). Coupled data assimilation for integrated Earth system analysis and prediction. *Bulletin of the American Meteorological Society*, *98*(7), ES169–ES172. https://doi.org/10.1175/BAMS-D-17-0036.1

Plaza Guingla, D. A., De Keyser, R., De Lannoy, G. J., Giustarini, L., Matgen, P., & Pauwels, V. R. (2013). Improving particle filters in rainfall-runoff models: Application of the resample-move step and the ensemble Gaussian particle filter. *Water Resources Research*, *49*(7), 4005–4021. https://doi.org/10.1002/wrcr.20291

Raanes, P. N. (2016). On the ensemble Rauch-Tung-Striebel smoother and its equivalence to the ensemble Kalman smoother. *Quarterly Journal of the Royal Meteorological Society*, *142*(696), 1259–1264. https://doi.org/10.1002/qj.2728

Rinaldo, A., Beven, K. J., Bertuzzo, E., Nicotina, L., Davies, J., Fiori, A., et al. (2011). Catchment travel time distributions and water flow in soils. *Water Resources Research*, *47*(7). https://doi.org/10.1029/2011WR010478

Royal Dutch Meteorological Institute (KNMI). (2023). KNMI climate data. Retrieved from https://www.daggegevens.knmi.nl/klimatologie/daggegevens

São Mateus, M. D. S. C., Machado, S. L., & Barbosa, M. C. (2012). An attempt to perform water balance in a Brazilian municipal solid waste landfill. *Waste Management*, *32*(3), 471–481. https://doi.org/10.1016/j.wasman.2011.11.009

Shockley, E. (2020). *A python implementation of the MT-DREAM(ZS) algorithm from Laloy and Vrugt 2012*. Online. Retrieved from https://github.com/LoLab-MSM/PyDREAM

Smith, P. J., Fowler, A. M., & Lawless, A. S. (2015). Exploring strategies for coupled 4d-var data assimilation using an idealised atmosphere–ocean model. *Tellus A: Dynamic Meteorology and Oceanography*, *67*(1), 27025. https://doi.org/10.3402/tellusa.v67.27025

Snyder, C., Bengtsson, T., Bickel, P., & Anderson, J. (2008). Obstacles to high-dimensional particle filtering. *Monthly Weather Review*, *136*(12), 4629–4640. https://doi.org/10.1175/2008MWR2529.1

Tardif, R., Hakim, G. J., & Snyder, C. (2015). Coupled atmosphere-ocean data assimilation experiments with a low-order model and CMIP5 model data. *Climate Dynamics*, *45*(5–6), 1415–1427. https://doi.org/10.1007/s00382-014-2390-3

Tran, V. N., Dwelle, M. C., Sargsyan, K., Ivanov, V. Y., & Kim, J. (2020). A novel modeling framework for computationally efficient and accurate real-time ensemble flood forecasting with uncertainty quantification. *Water Resources Research*, *56*(3), 1–31. https://doi.org/10.1029/2019WR025727

Van Leeuwen, P. J. (2009). Particle filtering in geophysical systems. *Monthly Weather Review*, *137*(12), 4089–4114. https://doi.org/10.1175/2009MWR2835.1

Vrugt, J. A. (2016). Markov chain Monte Carlo simulation using the dream software package: Theory, concepts, and matlab implementation. *Environmental Modelling & Software*, *75*, 273–316. https://doi.org/10.1016/j.envsoft.2015.08.013

Vrugt, J. A., ter Braak, C. J., Diks, C. G., & Schoups, G. (2013). Hydrologic data assimilation using particle Markov chain Monte Carlo simulation: Theory, concepts and applications. *Advances in Water Resources*, *51*, 457–478. https://doi.org/10.1016/j.advwatres.2012.04.002

Wang, L., & Heimovaara, J. (2024). Data and scripts underlying the manuscript: Quantifying landfill emission potential using a weakly coupled particle filter. *4TU.ResearchData*. https://doi.org/10.4121/1A723AEE-A309-43A3-8D62-1CB68BE6CFF6.V3

Weerts, A. H., & El Serafy, G. Y. (2006). Particle filtering and ensemble kalman filtering for state updating with hydrological conceptual rainfall-runoff models. *Water Resources Research*, *42*(9). https://doi.org/10.1029/2005WR004093

Yang, N., Damgaard, A., Kjeldsen, P., Shao, L.-M., & He, P.-J. (2015). Quantification of regional leachate variance from municipal solid waste landfills in China. *Waste Management*, *46*, 362–372. https://doi.org/10.1016/j.wasman.2015.09.016

Zhang, H., Hendricks Franssen, H.-J., Han, X., Vrugt, J. A., & Vereecken, H. (2017). State and parameter estimation of two land surface models using the ensemble Kalman filter and the particle filter. *Hydrology and Earth System Sciences*, *21*(9), 4927–4958. https://doi.org/10.5194/hess-21-4927-2017

Zhang, J., Zhang, J.-M., Xing, B., Liu, G.-D., & Liang, Y. (2021). Study on the effect of municipal solid landfills on groundwater by combining the models of variable leakage rate, leachate concentration, and contaminant solute transport. *Journal of Environmental Management*, *292*, 112815. https://doi.org/10.1016/j.jenvman.2021.112815

Zhang, S., Liu, Z., Zhang, X., Wu, X., Han, G., Zhao, Y., et al. (2020). Coupled data assimilation and parameter estimation in coupled ocean–atmosphere models: A review. *Climate Dynamics*, *54*(11–12), 5127–5144. https://doi.org/10.1007/s00382-020-05275-6

Županski, M. (2017). Data assimilation for coupled modeling systems. In S. K. Park & L. Xu (Eds.), *Data assimilation for atmospheric, oceanic and hydrologic applications* (Vol. III, pp. 55–70). Springer International Publishing. https://doi.org/10.1007/978-3-319-43415-5_2